Influence of Tool Dimension and Welding Parameters on Microstructure and Mechanical Properties of Friction-Stir-Welded 6061-T651 Aluminum Alloy

F.C. LIU and Z.Y. MA

Six-millimeter-thick 6061Al-T651 plates were friction stir welded with varied welding parameters and tool dimensions. The low hardness zones (LHZs), determined by constructing the hardness distribution maps around the heat-affected zones, changed the location and inclination with the welding conditions, but the hardness values of the LHZs were mainly dependent on the welding speed. The thermal cycles experienced by the LHZs had approximately the same peak temperature of 360 °C to 370 °C with varied durations that were governed by the welding speed. The microstructure of the LHZs was characterized by a low density of β' precipitates, which tended to reduce with increasing the welding speed. The fracture of the welds occurred along the LHZs, and the tensile strength of the welds increased with increasing the welding speed and was independent of the tool dimension and the rotation rate. A heat source zone-isothermal dissolution layer model was proposed to explain the observed effects.

DOI: 10.1007/s11661-008-9586-2

I. INTRODUCTION

FRICTION stir welding (FSW) is considered to be the most significant development in metal joining in recent years and is a "green" technology due to its energy efficiency, environment friendliness, and versatility.[1] This technique is being applied to the aerospace, automotive, and shipbuilding industries, and is attracting an increasing amount of research interests.

For the precipitation-hardened aluminum alloys, FSW creates a softened region in the heat-affected zone (HAZ) that has the lowest hardness within the entire weld, due to significant dissolution/coarsening of the precipitates during the FSW thermal cycle.[2–6] Therefore, the hardness profile of the FSW aluminum alloy joint is a direct indicator of microstructural evolution during FSW. In the previous studies, the hardness profiles were measured either along the midthickness of the FSW plate or along the top, center, and bottom of the plate thickness to determine the lowest hardness points.[1] However, it should pointed out that such hardness profiles could not predict the fracture behavior of FSW aluminum alloy joints because of the limited lowest hardness points.[1] In a recent study, Ren *et al.*[7] constructed a hardness distribution map around the HAZ throughout the entire thickness of 6-mm-thick FSW 6061Al-T651 plates. It was indicated that the fracture path of the welds was consistent with the lowest hardness distribution.

It is well documented that both welding parameters and tool geometry exert significant effects on the mechanical properties of the FSW aluminum alloy joints.[7–15] For example, Scialpi *et al.*[11] reported that the best FSW 6082Al joint was produced by a shoulder with fillet and cavity. However, the investigation by Fujii *et al.*[10] indicated that the tool shape did not affect the mechanical properties of FSW 6061Al-T651 joints significantly. However, they did not give a detailed explanation. On the other hand, the effect of the tool rotation rate or the welding speed on the mechanical properties of the FSW joints was examined by several investigators. Lee *et al.*[14] reported that both strength and elongation of FSW 6061Al-T651 joints decreased with decreasing the welding speed and increasing the rotation rate.[15] More recently, Ren *et al.*[7] reported that while the rotation rate did not influence the tensile properties of FSW 6061Al-T651 joints, increasing the welding speed increased the strength of the joints remarkably.

It was widely reported that the fracture of the FSW joints of the precipitation-strengthened aluminum alloys usually occurred in the HAZ. In this case, the mechanical properties of the welds are governed by the microstructure of the HAZ that is dominated by the thermal exposure during FSW thermal cycle. However, the previous investigations focused mainly on the microstructural examinations of the stir zone (SZ) and the temperature measurement at or near the SZ.[4,16–19] It is of practical importance to examine the thermal history and microstructural evolution of the HAZ and correlate the FSW conditions to the resultant mechanical properties of the welds.

A previous preliminary study has indicated that the fracture path of FSW 6061Al-T651 joints developed along the low hardness zone (LHZ), which was revealed

F.C. LIU, Postgraduate, and Z.Y. MA, Professor, are with the Shenyang National Laboratory for Materials Science, Institute of Metal Research, Chinese Academy of Sciences, Shenyang 110016, P.R. China. Contact e-mail: zyma@imr.ac.cn
Manuscript submitted December 24, 2007.
Article published online July 15, 2008

by constructing the hardness distribution map around the HAZ.[7] Therefore, it is worthwhile to examine the thermal history and microstructural evolution of the LHZ to understand the dominant influential factors. In this study, 6-mm-thick 6061Al-T651 plates were friction stir welded with different tool geometries under a wide range of FSW parameters, and the temperature profile of the LHZ was measured and the microstructure was examined. The aim is to (a) establish the relationship between the FSW conditions, the temperature profiles and microstructure of the LHZs, and the mechanical properties of the welds; (b) determine the dominant factor influencing the mechanical properties of the welds, and (c) establish a process model to explain the effects of the FSW parameter and tool geometry.

II. EXPERIMENTAL

The 6-mm-thick 6061Al-T651 rolled plate was used in this study. The chemical composition and the tensile properties of the plate were listed in Table I. This alloy has a balanced Mg to Si ratio (at. pct) of close to 2:1, corresponding to the stoichiometry of the Mg_2Si phase. The plates with a length of 400 mm and a width of 75 mm were butt welded along the rolling direction using a FSW machine (China FSW Center, Beijing, PR of China). The tools with the shoulders of 16, 20, and 24 mm in diameter and the threaded conical pins of 8 and 6 mm in root diameter were used. The FSW parameters used in this study were summarized in Table II. The FSW samples were designated using a series digital format. For example, sample 16-8-1400-400 denotes that the sample was welded by using a 16-mm-diameter shoulder and an 8-mm-diameter pin at a rotation rate of 1400 rpm and a welding speed of 400 mm/min.

After welding, the FSW samples were cross-sectioned perpendicular to the welding direction for microstructural examinations by optical microscopy (OM) and transmission electron microscopy (TEM, TECNAI20), hardness measurement, and tensile test. Metallographic samples were ground and polished to a colloidal 1-μm SiO_2 finish, and then were anodized in the Barker's solution (7.5 mL HBF_4, 75 mL H_2O_2, and 217 mL H_2O) at 25 V for 5 minutes. Grain structures were observed by OM under polarized light. The average grain size in the SZ was determined by the mean liner intercept technique (grain size = mean liner intercept × 1.78). Vickers microhardness was measured at an interval of 1 mm around the HAZ to determine the LHZs. The hardness measurement was conducted on an automatic testing machine (LECO,* LM-247AT) under a load of 300 g for 15 seconds. After the LHZs were obtained, the temperature profiles in the LHZs were recorded by embedding the thermocouples in the LHZs. The temperature data was sampled at an interval of 0.04 seconds by a temperature recorder. The configuration and size of the transverse tensile specimens are shown in Figure 1. Room-temperature tensile tests were carried out at a strain rate of 4×10^{-4} s^{-1} and the tensile properties of each condition reported were average of the results from three tests. The TEM foils were prepared by twin-jet electro polishing using a solution of 70 pct methanol and 30 pct nitric at 238 K and 19 V.

*LECO is a trademark of LECO Corporation, St. Joseph, MI.

III. RESULTS

A. *Microstructural Characteristics*

Figure 2 shows the cross-sectional macrostructures of the FSW 6061Al-T651 joints. Under investigated welding parameters, no welding defect was detected in the joints. Three microstructural zones, *i.e.*, stir zone (SZ), thermo-mechanically affected zone (TMAZ), and HAZ were discernible. The shapes of the SZ were apparently parameter dependent. The joint produced by a tool with a shoulder diameter of 16 mm exhibited a rectangular SZ with an incomplete onion ring structure (Figure 2(a)). With increasing the shoulder diameter, the SZ changed from rectangular to elliptical, and the center of the onion rings shifted downward from the upper part of the SZ (Figures 2(a) through (c)). With increasing the welding speed from 400 to 600 mm/min, the center of the onion rings shifted from the middle of the SZ to the upper part, whereas with decreasing the welding speed from 400 to 200 mm/min, the onion ring structure disappeared (Figures 2(c) through (e)). For a lower welding speed of 200 mm/min, decreasing the tool rotation rate from 1400 to 900 rpm eliminated the nugget boundary at the retreating side (Figures 2(e) through (g)). When the pin diameter decreased from 8 to 6 mm, the size of the SZ decreased obviously (Figures 2(b) and (h)).

Figure 3 shows the OM micrographs of the base material (BM), HAZ, TMAZ, and SZ of sample 24-8-1400-400. Both the BM and the HAZ were characterized by the elongated grains resulting from the rolling process, and no distinct difference was discernible between them (Figures 3(a) and (b)). These grains are several hundred microns long and approximately 80-μm wide. The elongated grains were deformed in an upward flowing pattern in the TMAZ, as shown in Figure 3(c). Although the TMAZ underwent plastic deformation, recrystallization did not occur in this zone due to insufficient deformation strain and thermal input. The SZ exhibited fine and equiaxed grain structure with an average grain size of ~12 μm, indicating the occurrence of dynamic recrystallization due to severe plastic deformation and thermal exposure (Figure 3(d)).

In order to evaluate the precipitate distribution in the HAZ of the FSW 6061Al-T651 joints and correlate the local thermal cycle with the hardness distribution, the HAZ was plotted out as three subzones, *i.e.*, HAZ I, HAZ II, and HAZ III, as shown in Figure 2(c). HAZ II corresponds to the LHZ of the hardness distribution map, as will be discussed in Section III–B. It should be pointed out that the authors are not trying to change or

Table I. Chemical Compositions and Mechanical Properties of 6061Al-T651 Rolled Plate

Chemical Composition (Wt Pct)						Mechanical Properties		
Mg	Si	Fe	Cu	Zn	Mn	UTS, MPa	YS, MPa	El., Pct
0.6 to 1.2	0.4 to 0.8	0.7	0.15 to 0.40	0.25	0.15	308	285	18

Table II. Welding Parameters and Designations of FSW 6061Al-T651 Samples

Sample	Shoulder Diameter (mm)	Pin Diameter (mm)	Rotation Rate (ω), rpm	Welding Speed (v), mm/min	Designation
1	16	8	1400	400	16-8-1400-400
2	20	8	1400	400	20-8-1400-400
3	24	8	1400	400	24-8-1400-400
4	24	8	1400	600	24-8-1400-600
5	24	8	1400	200	24-8-1400-200
6	24	8	1200	200	24-8-1200-200
7	24	8	900	200	24-8-900-200
8	20	6	1400	400	20-6-1400-400

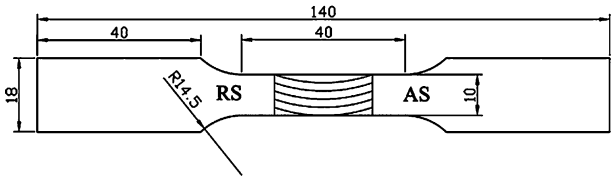

Fig. 1—Configuration and size of tensile specimens.

complicate the existing nomenclature for FSW, but will use HAZ I, II, and III only for convenience in this manuscript.

Figure 4 shows TEM images of the three subzones of the HAZ of sample 24-8-1400-400. The incident electron beam is parallel to a ⟨100⟩ zone axis of the matrix in each micrograph. HAZ I was characterized by a comparatively high density of needle-shaped precipitates and few rod-shaped precipitates (Figure 4(a)). HAZ II contained only a low density of rod-shaped precipitates (Figure 4(b)). In HAZ III, both types of the precipitates disappeared fundamentally (Figure 4(c)).

Figures 5(a) and (b) show the precipitates in HAZ II of samples 24-8-1400-200 and 24-8-1400-600, respectively. The fine needle-shaped precipitates had dissolved fundamentally, and only low density of the rod-shaped precipitates remained in both samples. With increasing the welding speed from 200 to 600 mm/min, the rod-shaped precipitates tended to reduce (Figures 5(a), 4(b), and 5(b)).

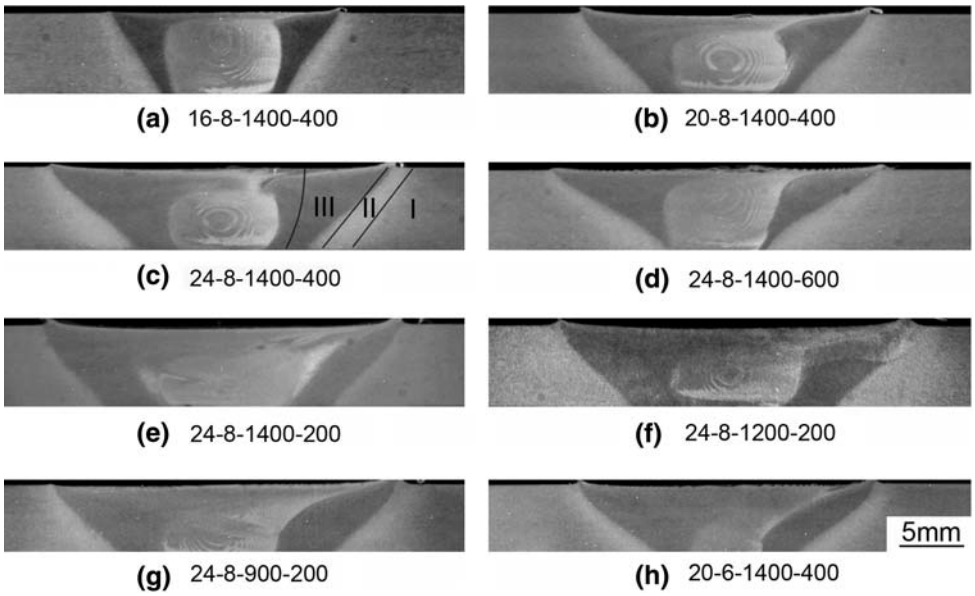

Fig. 2—Cross-sectional macrostructures of FSW 6061Al-T651 joints.

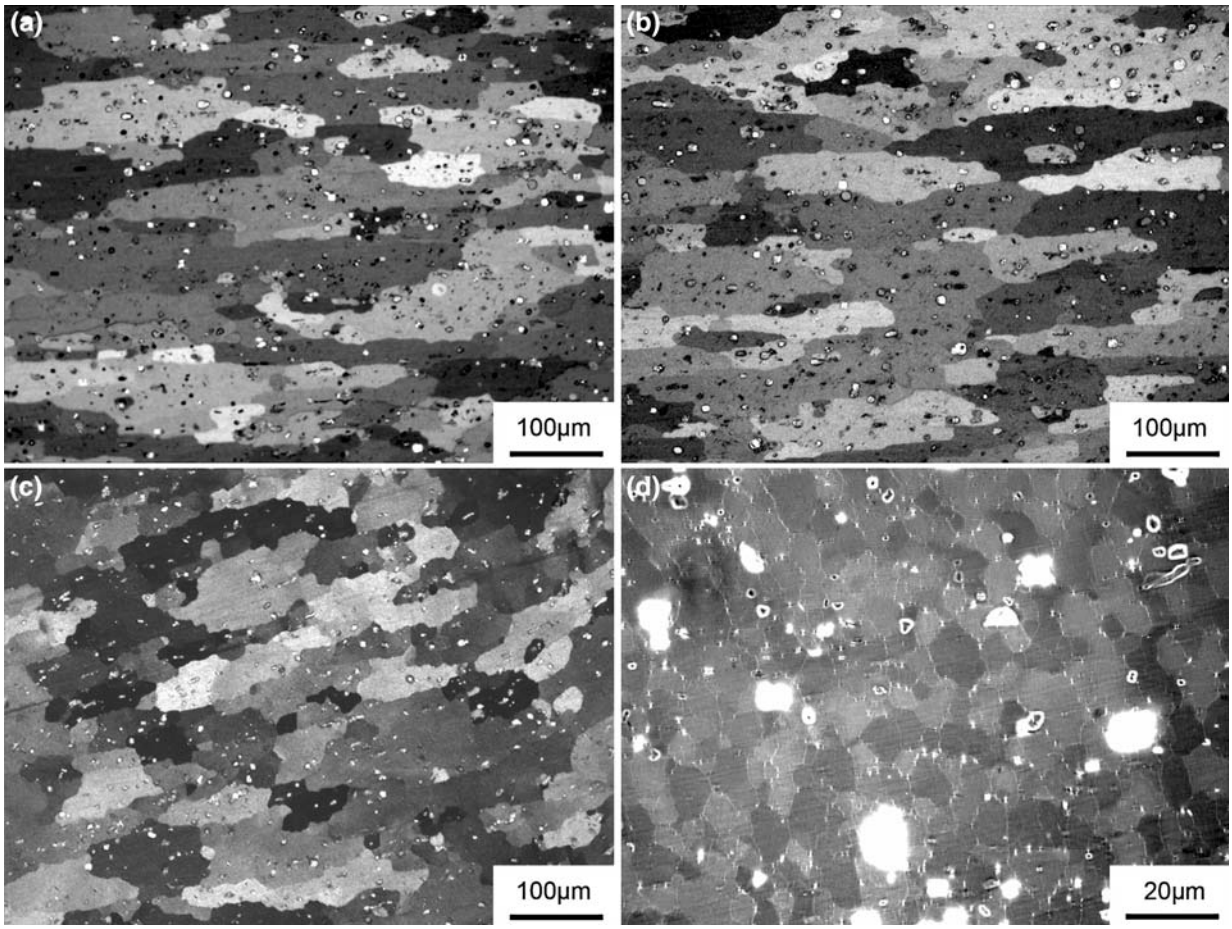

Fig. 3—Optical micrograph of sample 24-8-1400-400: (*a*) BM, (*b*) HAZ, (*c*) TMAZ, and (*d*) SZ.

B. *Microhardness Map*

The hardness distribution maps of the FSW 6061Al-T651 samples around the HAZ are shown in Figure 6. The LHZs were observed to exhibit a ~30 to 45 deg angle to the butting surface under different FSW conditions. Four important observations can be made. First, for the same FSW parameters and pin design, the LHZs moved outward relative to the weld center with increasing the shoulder diameter from 16 to 24 mm (Figures 6(a) through (c)). Further, the inclination of the LHZs to the butting surface tended to increase with increasing the shoulder diameter. However, the hardness values along the LHZs are similar (~65 to 70 Hv) for all three welds. Second, for the same tool geometry and tool rotation rate, with increasing the welding speed from 200 to 600 mm/min, the distance of the LHZs to the weld center decreased and the inclination of the LHZs to the butting surface increased from ~30 to ~45 deg (Figures 6(c) through (e)). Further, the hardness values along the LHZs increased from ~57 to 62, to ~69 to 75 Hv with increasing the welding speed. Third, for the same tool geometry and welding speed, increasing the tool rotation rate from 900 to 1400 rpm resulted in a movement of ~4 mm in the LHZs outward relative to the weld center. However, the LHZs exhibited similar hardness values of ~57 to 62 Hv and inclination of ~30 deg to the butting surface (Figures 6(e) through (g)). Fourth, with the same shoulder and FSW parameters, decreasing the pin diameter from 8 to 6 mm exerted no noticeable effect on the location, inclination, and hardness value of the LHZs (Figures 6(b) and (h)).

C. *Thermal Cycle*

Figure 7 shows the temperature history recorded at different locations on the LHZs of sample 24-8-1400-400. Profiles 1 and 2 correspond to the thermal cycles of locations 1 and 2, respectively, as shown in Figure 8. The two locations experienced approximately the same thermal cycle, especially at higher temperature range.

Figure 9 shows the temperature history of the LHZs during FSW recorded at location 2 for various welds, as shown in Figure 8. The LHZs of all the welds experienced the approximately same peak temperatures of 360 °C to 370 °C. However, a close examination on Figure 9 reveals the following important observations. First, the duration of the thermal cycles at higher temperatures of >250 °C was shortened with increasing the welding speed from 200 to 600 mm/min (cycles A, B, and F). Second, increasing the shoulder diameter from 16 to 24 mm (cycles B, C, and D) did not change the duration of the thermal cycles above 250 °C fundamentally.

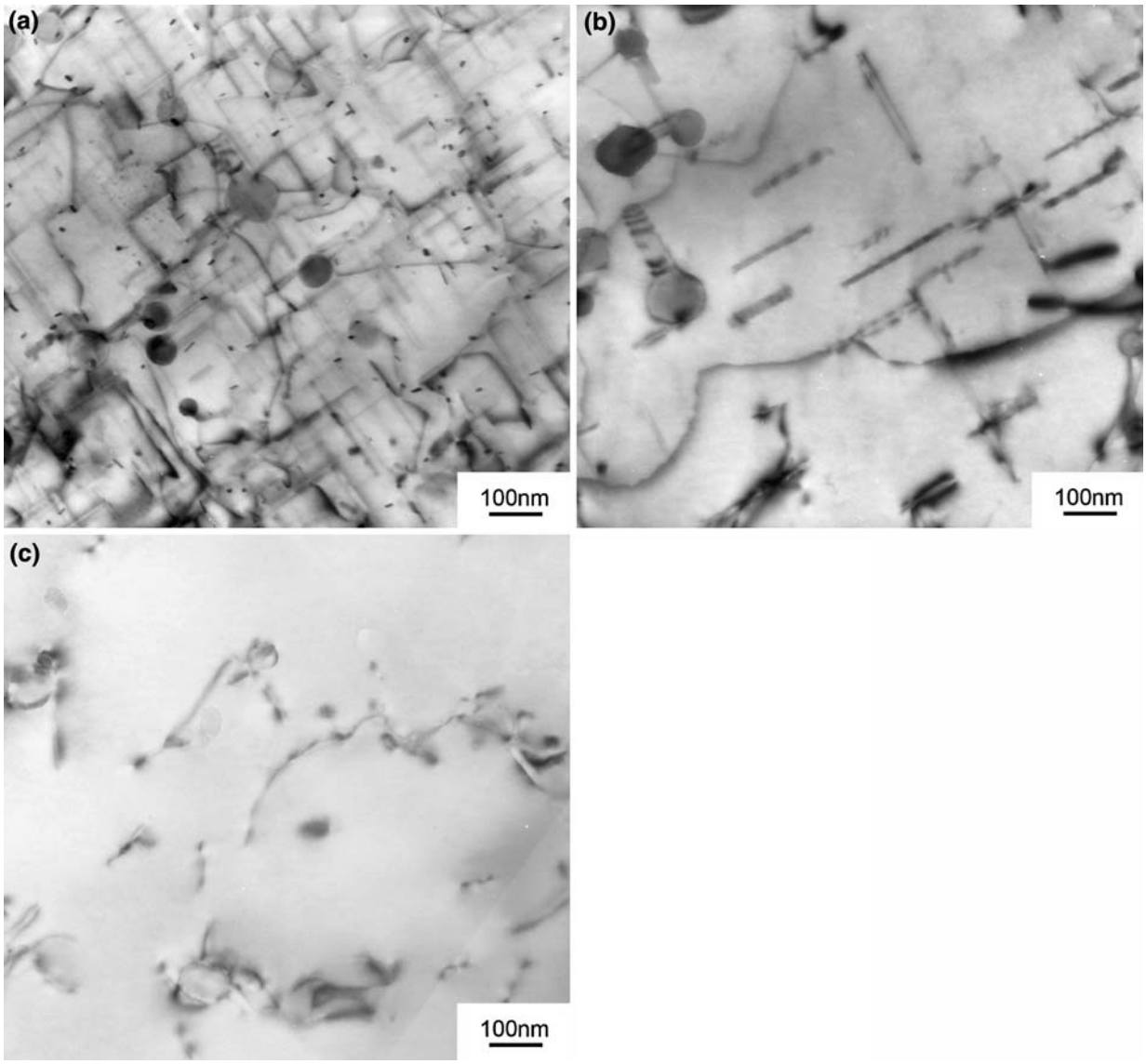

Fig. 4—Bright-field TEM micrographs of (*a*) HAZ I, (*b*) HAZ II, and (*c*) HAZ III of sample 24-8-1400-400, as shown in Fig. 2(c).

Third, under a constant welding speed of 200 mm/min, increasing the rotation rate from 900 to 1400 rpm (cycles E and F) exerted no noticeable effect on the duration of the thermal cycles above 250 °C.

D. *Tensile Properties*

Figure 10 shows the failed tensile specimens. The weld centerline for each of the specimens was marked. All of the welds exhibited the similar shear fracture pattern with the failure occurring in the HAZ and with limited necking (Figure 10). The shear fracture path was a ~45 to 60 deg angle to the tensile axis. The fracture position and fracture path correspond roughly with the LHZs (Figure 6).

The tensile properties of the FSW 6061Al-T651 joints are shown in Table III. Table III reveals four important findings. First, all the welds exhibited a similar elongation despite FSW parameters and tool dimension. Second, under the same FSW parameters, increasing the shoulder diameter from 16 to 24 mm or the pin diameter from 6 to 8 mm did not produce a noticeable effect on the tensile strength of the welds. Third, for the same tool geometry and tool rotation rate, the tensile strength increased with increasing the welding speed from 200 to 600 mm/min. Fourth, for the same tool dimension and a constant welding speed of 200 mm/min, increasing the tool rotation rate from 900 to 1400 rpm did not change the strength of the welds.

IV. DISCUSSION

A. *Temperature Distribution*

The temperature measurement revealed that the two locations at the same LHZ experienced approximately the same thermal cycle (Figure 7). Examining the

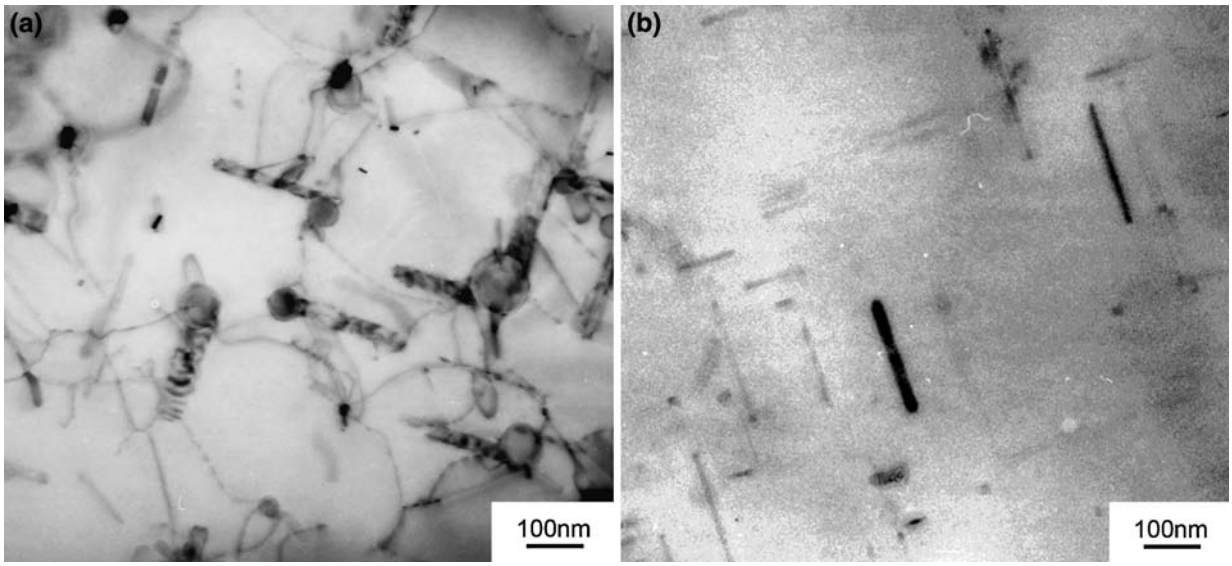

Fig. 5—Bright-field TEM micrographs showing rod-shaped precipitates in HAZ II: (*a*) sample 24-8-1400-200 and (*b*) sample 24-8-1400-600.

hardness values along the LHZs, it was found that the hardness values, which are the indicators of the thermal input, were approximately constant along each LHZ (Figure 6). Combining the results of the hardness and temperature, we can conclude that the entire LHZ experienced approximately the same thermal cycle during FSW.

Tang *et al.*[17] measured the temperature distribution within the welds by embedding thermocouples in the region to be welded. It was reported that increasing the tool rotation rate resulted in an increase in the weld temperature. Similarly, Kwon *et al.*[18] and Sato *et al.*[19] also indicated that the peak temperature in the weld zone increased with increasing the rotation rate. On the other hand, Frigaad *et al.*[20] revealed that the peak temperature decreased with increasing the welding speeds from 300 to 720 mm/min. A peak temperature of up to 550 °C has been recorded in the region adjacent to the SZ.[21] It should be pointed out that although a lot of effort has been made to determine the peak temperature in or near the SZ, the temperature history in the HAZ has been rarely recorded.[4,16,22] This study has indicated that the LHZs in various welds experienced approximately the same peak temperature of 360 °C to 370 °C during the FSW thermal cycles, irrespective of the FSW parameters and tool dimensions.

Sato *et al.*[4] examined the microstructural evolution of 6063Al-T5 during FSW. By comparing the microstructures in various regions of the weld to those in the base material that was subjected to simulated weld thermal cycles with different peak temperatures, the relationship between the peak temperature of the FSW thermal cycle and the microstructure of the weld was established. It was shown that the precipitate distribution in the 6063Al was not effectively influenced by the thermal cycle with a peak temperature of lower than 201 °C. For the thermal cycle with the peak temperature of 252 °C to 353 °C, the density of the needle-shaped precipitates decreased with the increase in the peak temperature. When the peak temperature was higher than 402 °C, the thermal cycle led to the dissolution of all the precipitates. The peak temperature of the minimum hardness region was estimated to be 353 °C.[4] The peak temperature of 360 °C to 370 °C measured in the LHZs of the FSW 6061Al joints by the thermocouples in this study is in good agreement with that estimated through simulated weld thermal cycles by Sato *et al.*[4]

In the present study, as shown in Figure 9, the overaging time "$t = t_1 + t_2$" is defined as the entire time for increasing the temperature from 250 °C to the peak temperature (t_1) followed by cooling to 250 °C (t_2). The heating and cooling rates are defined as T_1/t_1 and T_1/t_2, respectively. The term T_1 is the increment of temperature from 250 °C to the peak temperature. The selection of the temperature range T_1 is because the thermal cycle above 250 °C resulted in the dissolution of the needle-shaped precipitates in the Al-Mg-Si alloy.[4] Therefore, the overaging time is hereafter termed as the dissolution time.

For cycle A with a welding speed of 600 mm/min, the heating and cooling rates were 80 °C/s and 40 °C/s, respectively, and the dissolution time was only 4.5 seconds. For cycles B through D with a welding speed of 400 mm/min, the heating and cooling rates were 45 °C to 50 °C/s and 25 °C to 28 °C/s, respectively, and the dissolution time increased to 6.5 to 7.5 seconds. For cycles E and F with a welding speed of 200 mm/min, the heating and cooling rates were 30 °C/s to 33 °C/s and 12 °C/s to 13 °C/s, respectively, and the dissolution time increased to 13 to 14 seconds. Considering the fact that cycles B through D had different shoulder dimensions and cycles E and F had different rotation rates, it is clear that the dissolution time in the LHZs was not dependent on the shoulder dimension and the rotation rate, but governed by the welding speed, and decreased with

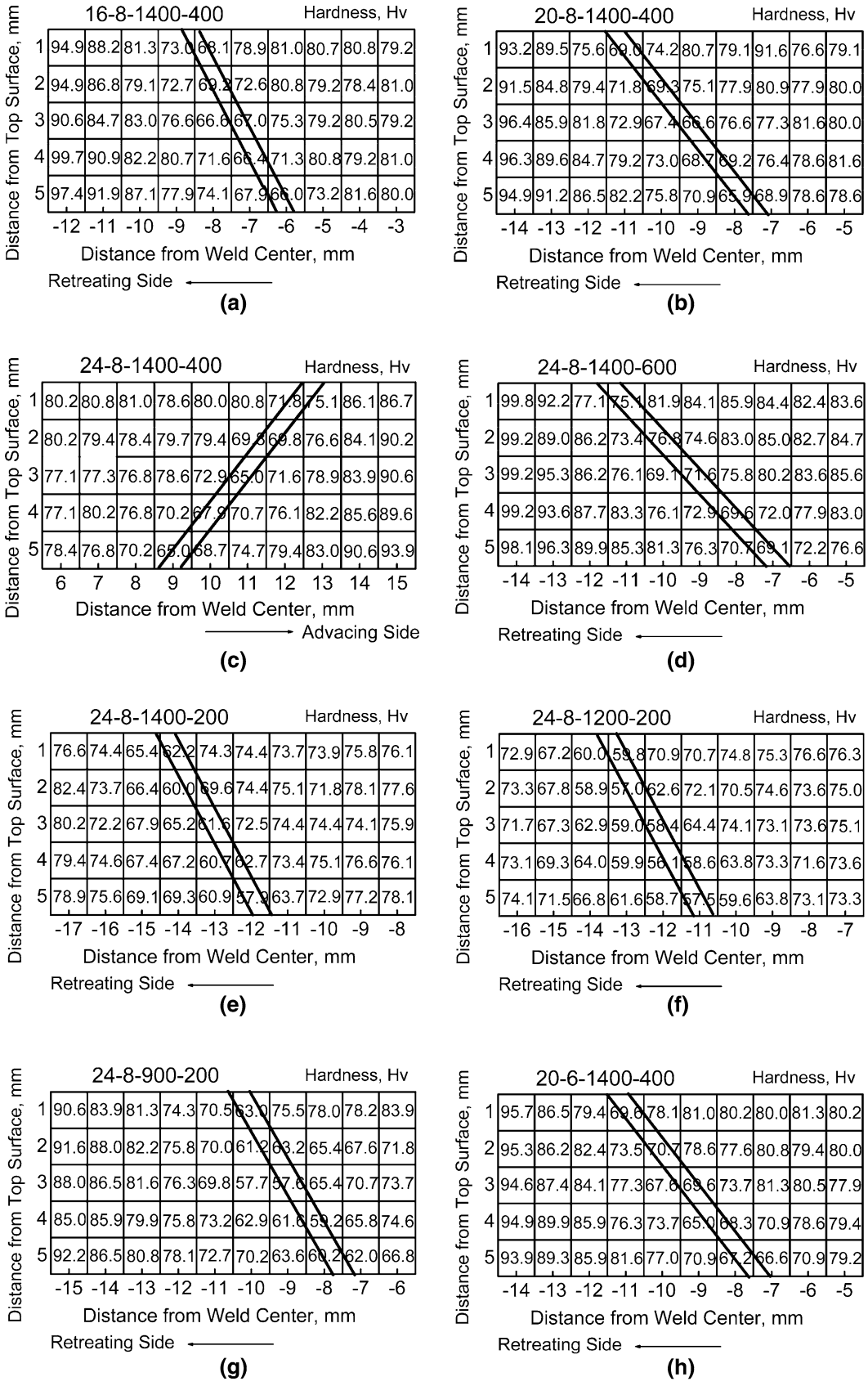

Fig. 6—Microhardness distribution maps of FSW 6061Al-T651 joints around HAZ.

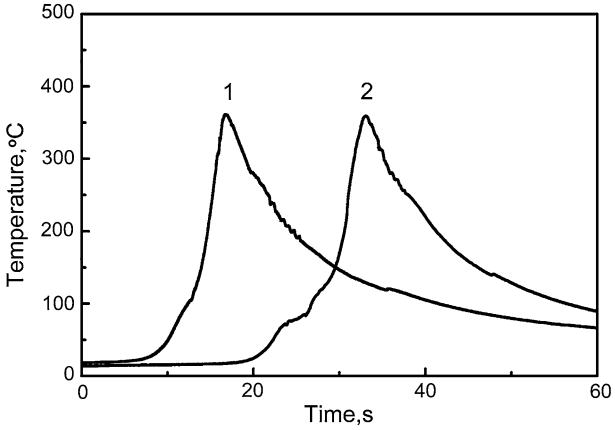

Fig. 7—Temperature histories recorded at two different locations of LHZ for sample 24-8-1400-400 (locations 1 and 2 were 5 and 3 mm from top surface, as shown in Fig. 8).

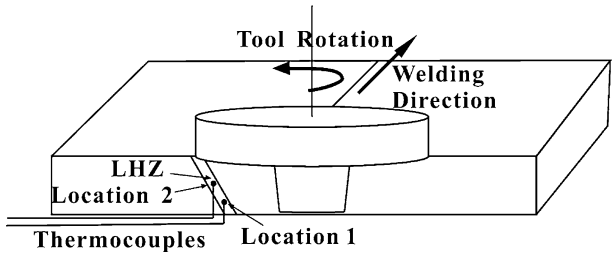

Fig. 8—Schematic of locations where thermocouples were embedded.

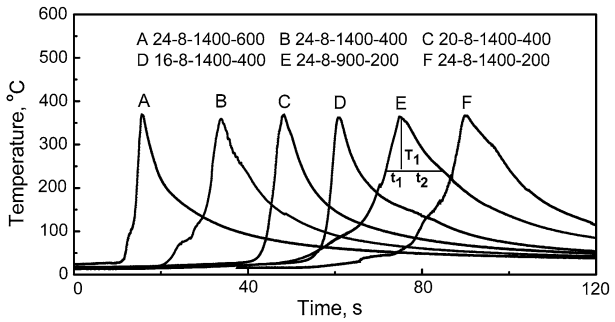

Fig. 9—Temperature histories recorded at LHZs for various welds.

increasing the welding speed. These observations will be explained by the heat source zone-isothermal dissolution layer model in Section C.

B. *Precipitate Evolution*

It is well documented that the precipitation sequence of the Al-Mg-Si alloys during aging is supersaturated solid solution → needle-shaped precipitate → β' precipitate → β-Mg_2Si.[23–28] The β' precipitates were featured as the coarse rods of approximately 50 to 700 nm in length.[28,29] This suggests that the rod-shaped precipitates of around 100 nm in length in the present FSW 6061Al joints are the β' phase (Figures 4 and 5). The fine needle-shaped precipitates of less than 50 nm in length are defined as the GP zones/β'' in many previous studies.[25–28] However, some studies indicated that these precipitates have different crystallographic structures.[30–33] Because no acceptable electron diffraction patterns could be obtained from the precipitates in this study, the precipitates of less than 50 nm in size were considered to be the needle-shaped precipitates on the basis of previous studies.[23–33]

The precipitates in the HAZ are dominantly influenced by the temperature distribution. In this study, the HAZ was plotted out as three subzones, *i.e.*, HAZ I, HAZ II, and HAZ III (Figure 2(c)). HAZ II experienced a thermal cycle with a medium peak temperature of 360 °C to 370 °C. Only a low density of the rod-shaped precipitates were observed in HAZ II (Figure 4(b)), leading to the generation of the LHZ in the joint (Figure 6). In HAZ I, which experienced a low-peak-temperature thermal cycle due to being far from the SZ, the existence of the needle-shaped precipitates made it have a higher hardness than HAZ II (Figures 4(a) and 6). In HAZ III, which experienced a high-peak-temperature thermal cycle due to being near the SZ, almost all precipitates dissolved into the aluminum matrix (Figure 4(c)), resulting in the enhanced effect of solution strengthening in HAZ III. In this case, the hardness of HAZ III was higher than that of HAZ II (Figure 6).

It was previously reported that some of the needle-shaped precipitates grew into the β' precipitates, whereas some of the needle-shaped precipitates dissolved during FSW of 6063Al.[4] The growth and dissolution of the needle-shaped precipitates are determined by the heating and cooling rates, peak temperature, and dissolution time. The present study indicates that the FSW thermal cycles with different welding speeds underwent approximately the same peak temperature, but different heating and cooling rates, and dissolution times. When the welding speed increased from 200 to 600 mm/min, the heating and cooling rates increased and the dissolution time decreased, resulting in the decrease in both the density and dimension of the β' precipitates (Figures 4(b) and 5).

C. *Heat Source Zone–Isothermal Dissolution Layer Model*

The heat input during FSW was generally considered to be the result of friction between the rotating tool and the welded plates and the plastic deformation work of the central weld zone. When the welding tool moved along the joint line, no plastic deformation, induced by the mechanical stirring, took place in the HAZ. The HAZ only experienced a thermal exposure. Thus, when we evaluate the effect of FSW on the HAZ, a zone located just below the shoulder of the tool with a shape of inverted trapezoidal, as shown in Figure 11, can be regarded as the heat source zone (HSZ). During FSW, as the HSZ with a high temperature moved along the joint line at a given speed, a thermal exposure was exerted to the material around the HSZ and resulted in the generation of the LHZs that experienced a thermal cycle with approximately the same peak temperature of

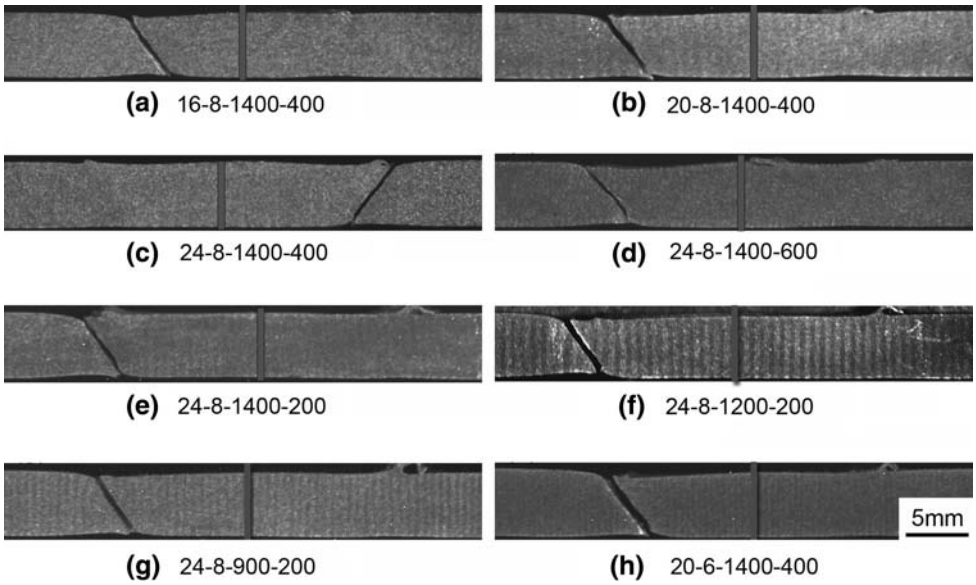

Fig. 10—Appearance of failed FSW 6061Al-T651 joints.

Table III. Transverse Tensile Properties of FSW 6061Al-T651 Joints

Designation	UTS, MPa	El., Pct	UTS_{FSW}/UTS_{base}
16-8-1400-400	231	8.1	0.75
20-8-1400-400	229	8.4	0.74
24-8-1400-400	230	8.3	0.75
24-8-1400-600	243	8.6	0.79
24-8-1400-200	214	8.8	0.69
24-8-1200-200	211	8.6	0.69
24-8-900-200	214	8.4	0.69
20-6-1400-400	230	8.2	0.75

360 °C to 370 °C. In this case, the LHZs are defined as the isothermal dissolution layers (ITDLs), which correspond to the temperature range for the dissolution of the needle-shaped precipitates, as discussed previously.

Chen and Kovacevic[22] have shown a temperature distribution along the lateral direction at the instant when the tool is traversing this cross section. It was indicated that the isothermal nodes moved away from the joint line with the increase of the peak temperature in the SZ. Thus, in this study, when the temperature of the HSZ increased due to increased tool rotation rates and shoulder diameters and decreased welding speeds, the ITDLs with a temperature of 360 °C to 370 °C moved away from the HSZ. For a constant welding speed, the ITDLs experienced approximately the same local thermal cycle, *i.e.*, a same dissolution time. However, when the welding speed increased, the dissolution time experienced by the ITDLs decreased.

D. *Hardness Distribution*

Different from the previous studies, where a one or three horizontal hardness profile was measured either along the midthickness of the FSW plate or along the top, center, and bottom of the plate thickness,[1] in this study, the hardness distribution map was constructed around the HAZ by measuring the microhardness at an interval of 1 mm. From such a hardness distribution map, a LHZ was easily determined, as shown by the straight lines in Figure 6, due to the distinct hardness difference between the LHZ and the adjacent regions. Increasing the shoulder diameter from 16 to 24 mm resulted in an outward movement of the LHZs relative to the weld center and an increase in the inclination of the LHZs to the butting surface. However, the hardness values of the LHZs did not change fundamentally. This is because these LHZs experienced approximately the

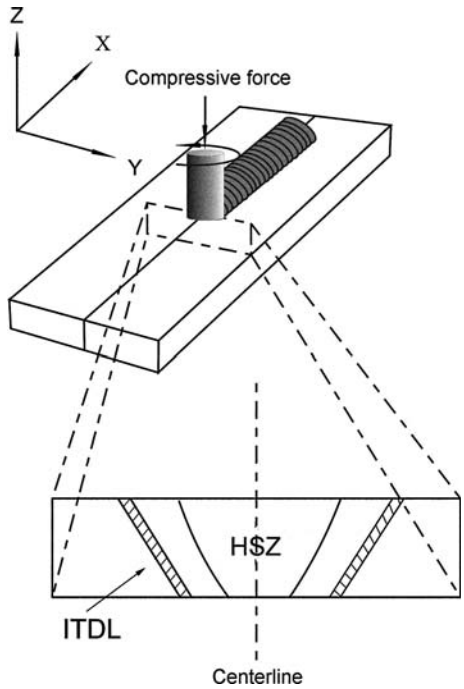

Fig. 11—Schematic of HSZ-ITDL model.

same thermal cycle with a peak temperature of 360 °C to 370 °C and a dissolution time of 6.5 to 7.5 seconds, as shown by cycles B, C, and D in Figure 9. Similarly, increasing the rotation rate did not affect the hardness values of the LHZs due to quite similar thermal profiles, though the position of the LHZs was moved outward. By comparison, increasing the welding speed from 200 to 600 rpm not only changed the position and inclination of the LHZs, but also increased the hardness values of the LHZs obviously. This is attributed to remarkably shortened dissolution time (from 4.5 to 13 to 14 seconds), as discussed in Section A. The increase in the inclination of the LHZ with respect to the butting surface with increasing the welding speed is mainly attributed to the increased temperature difference between the top and the bottom of the plate.

E. *Tensile Properties*

For the FSW joints of the precipitation-strengthened aluminum alloys, the fracture of the transverse tensile specimens occurred at the HAZ, *i.e.*, the weakest zone of the joint.[11,16,17] A previous study has indicated that the fracture path of the FSW 6061Al joints was consistent with the distribution of the lowest hardness.[7] In this study, all the tensile specimens failed roughly along the LHZs, and the tensile strength of the welds corresponded well with the hardness values along the LHZs. This demonstrates that while the fracture location and inclination to the tensile axis of the FSW 6061Al-T651 joints were controlled by the position and inclination of the LHZs, the tensile strength was determined by the hardness values along the LHZs. For a constant welding speed, the welds exhibited almost the same tensile strengths, in spite of the diameter of the shoulder and pin and the tool rotation rate. With increasing the welding speed from 200 to 600 mm/min, the tensile strength of the welds increased (Table III).

F. *Practical Implication*

The results of this study are significant. It is indicated that the mechanical properties of the FSW joints of the peak-aged aluminum alloys can be improved by using two routes. The first is to increase the welding speed, thereby shortening the dissolution time for the precipitates in the ITDLs. In this case, the dissolution of the precipitates in the HAZ, such as the needle-shaped precipitates in the Al-Mg-Si alloys, can be significantly reduced. The second is to reduce the temperature of the HSZ by decreasing the FSW heat input, so that the temperature of the HAZ is lower than that for the dissolution of the precipitates. Thus, the ITDL that corresponds to the dissolution temperature for the precipitates is eliminated, thereby resulting in an improvement in the mechanical properties of the welds.

V. CONCLUSIONS

1. Defect-free FSW 6061Al-T651 joints were produced under a wide range of FSW parameters and tool dimensions. The grain shape and size did not change significantly from the BM to the HAZ.
2. The LHZs with an inclination of ~30 to 45 deg angle to the butting surface were determined by constructing the hardness distribution maps around the HAZ. The change in the shoulder and pin diameters and the rotation rate changed the position and inclination of the LHZs, but did not affect the hardness values along the LHZs. Increasing the welding speed increased the hardness values along the LHZs.
3. All the thermal cycles experienced by the LHZs exhibited approximately the same peak temperature of 360 °C to 370 °C. Increasing the welding speed increased the heating and cooling rates and reduced the dissolution time of the needle-shaped precipitates. However, the change in the shoulder and pin diameter and the tool rotation rate did not exert a noticeable effect on the heating and cooling rates and the dissolution time.
4. A low density of the β' precipitates was observed in the LHZs, which led to the generation of the minimum hardness in the joint. The β' precipitates in the LHZs tended to be reduced with an increase in the welding speed.
5. The tensile strength of the FSW 6061Al-T651 joints increased with increasing the welding speed and was independent of the dimension of the shoulder and pin and the rotation rate, and the fracture occurred along the LHZs. These were consistent with the position/inclination and the hardness values of the LHZs.
6. The effect of the FSW parameter and tool dimension on the thermal profile, microstructural evolution, strength, and fracture behavior can be reasonably explained by a heat source zone-isothermal dissolution layer model.

ACKNOWLEDGMENTS

The author gratefully acknowledges the support of (a) the National Outstanding Young Scientist Foundation with Grant No. 50525103 and (b) the Hundred Talents Program of the Chinese Academy of Sciences.

REFERENCES

1. R.S. Mishra and Z.Y. Ma: *Mater. Sci. Eng. R*, 2005, vol. 50, pp. 1–78.
2. G. Liu, L.E. Murr, C.S. Niou, J.C. McClure, and F.R. Vega: *Scripta Mater.*, 1997, vol. 37, pp. 355–61.
3. S. Lim, S. Kim, C.G. Lee, and S. Kim: *Metall. Mater. Trans. A*, 2004, vol. 35A, pp. 2837–43.
4. Y.S. Sato, H. Kokawa, M. Enmoto, and S. Jogan: *Metall. Mater. Trans. A*, 1999, vol. 30A, pp. 2429–37.
5. Y.S. Sato, H. Kokawa, M. Enmoto, S. Jogan, and T. Hashimoto: *Metall. Mater. Trans. A*, 1999, vol. 30A, pp. 3125–30.
6. Y.S. Sato, H. Kokawa, M. Enmoto, S. Jogan, and T. Hashimoto: *Metall. Mater. Trans. A*, 2001, vol. 32A, pp. 941–48.
7. S.R. Ren, Z.Y. Ma, and L.Q. Chen: *Scripta Mater.*, 2007, vol. 56, pp. 69–72.

8. M. Boz and A. Kurt: *T. Mater. Design*, 2004, vol. 26, pp. 343–47.
9. P. Cavaliere, G. Campanile, F. Panella, and A. Squillace: *J. Mater. Process. Tech.*, 2006, vol. 5, pp. 263–70.
10. H. Fujii, L. Cui, M. Maeda, and K. Nogi: *Mater. Sci. Eng. A*, 2006, vol. A419, pp. 25–31.
11. A. Scialpi, L.A.C. De Filippis, and P. Cavaliere: *Mater. Des.*, 2007, vol. 28, pp. 1124–29.
12. M. Jariyaboon, A.J. Davenport, R. Ambat, B.J. Connolly, S.W. Williams, and D.A. Price: *Corr. Sci.*, 2007, vol. 49, pp. 877–909.
13. S. Wei, C.Y. Hao, and J.C. Chen: *Mater. Sci. Eng. A*, 2007, vols. A452–A453, pp. 170–77.
14. W.B. Lee, Y.M. Yeon, and S.B. Jung: *Mater. Trans.*, 2004, vol. 45, pp. 1700–05.
15. S. Lim, S. Kim, C. Lee, C.G. Lee, and S. Kim: *Metall. Mater. Trans. A*, 2004, vol. 35A, pp. 2829–35.
16. M.W. Mahoney, C.G. Rhodes, J.G. Flintoff, R.A. Spurling, and W.H. Bingle: *Metall. Mater. Trans. A*, 1998, vol. 29A, pp. 1955–64.
17. W. Tang, X. Guo, J.C. McClure, and L.E. Murr: *J. Mater. Process. Manufact. Sci.*, 1998, vol. 7, pp. 163–72.
18. Y.J. Kwon, N. Saito, and I. Shigematsu: *J. Mater. Sci. Lett.*, 2002, vol. 21, pp. 1473–76.
19. Y.S. Sato, M. Urata, and H. Kokawa: *Metall. Mater. Trans. A*, 2002, vol. 33A, pp. 625–35.
20. O. Frigaad, O. Grong, and O.T. Midling: *Metall. Mater. Trans. A*, 2001, vol. 32A, pp. 1189–200.
21. T. Hashimoto, S. Jyogan, K. Nakata, Y.G. Kim, and M. Ushio: *Proc. 1st Int. Symp. on Friction Stir Welding*, Thousand Oaks, CA, June 14–16, 1999.
22. C.M. Chen and R. Kovacevic: *Int. J. Mach. Tool. Manu.*, 2003, vol. 44, pp. 1205–14.
23. K. Ohori: *J. Jpn Inst. Light Met.*, 1988, vol. 38, pp. 748–63.
24. C.E. Cross and G.R. Edwards: in *Treatise on Materials Science and Technology*, vol. 31, *Aluminum Alloys–Contemporary Research and Applications*, A.K. Vasudevam and R.D. Doherty, eds., Academic Press, New York, NY, 1989, pp. 53–54.
25. N. Maruyama, R. Uemori, N. Hashimoto, M. Saga, and M. Kikuchi: *Scripta Mater.*, 1997, vol. 36, pp. 89–93.
26. S. Ceresara, E. Dirusso, P. Fiorini, and A. Giarda: *Mater. Sci. Eng.*, 1970, vol. 5, pp. 220–27.
27. M.H. Jacobs: *Phil. Mag.*, 1972, vol. 26, pp. 1–13.
28. I. Dutta and S.M. Allen: *J. Mater. Sci. Lett.*, 1991, vol. 10, pp. 323–26.
29. M. Peel, A. Steuwer, M. Preuss, and P.J. Withers: *Acta Mater.*, 2003, vol. 51, pp. 4791–4801.
30. K. Matsuda, S. Ikeno, and S. Tada: *J. Jpn. Inst. Metall.*, 1993, vol. 57, pp. 1107–13.
31. K. Matsuda, S. Ikeno, T. Sato, and A. Kamio: *Scripta Mater.*, 1996, vol. 34, pp. 1797–1802.
32. K. Matsuda, H. Gamada, K. Fujii, T. Yoshida, T. Sato, A. Kamio, and S. Ikeno: *J. Jpn. Inst. Light Metall.*, 1997, vol. 47, pp. 493–99.
33. K. Matsuda, T. Yoshida, H. Gamada, K. Fujii, Y. Uetani, T. Sato, A. Kamio, and S. Ikeno: *J. Jpn. Inst. Metall.*, 1998, vol. 62, pp. 133–39.